THE ASTRONOMICAL JOURNAL VOLUME 92, NUMBER 2 FEBRUARY 1987

A PHOTOMETRIC SURVEY OF THE RICH OB ASSOCIATION NGC 206 IN M31

STEPHEN ODEWAHN
McDonald Observatory, University of Texas, Austin, Texas 78712
Received 9 September 1986

ABSTRACT

An extensive *UBV* photometric survey of the stellar content of the massive OB association NGC 206 has been conducted with the Griboval electronographic camera and a CCD camera attached to the $f/13$ focus of the 76 cm reflector of McDonald Observatory. After a detailed evaluation of the photometric errors, a catalog of weighted mean B band magnitudes complete to $B = 19.5$ was obtained, from which a differential luminosity function has been constructed. A B band absorption value of $A_B = 1.15 \pm 0.1$, derived by three independent methods, and a geometric distance modulus of $\mu_0 = 24.07$, were used to transform this luminosity function to an absolute scale. A method requiring only photometric data was utilized in computing the stellar mass frequency distribution in NGC 206 for the mass range between 20 and $60\mathscr{M}_\odot$. Assuming a constant stellar birthrate, a straightforward computation of the initial mass function was performed. The significant effects of mass loss and convective overshoot were accounted for in the mass-luminosity relation and stellar ages used in the transformation. A power law fit to the derived IMF gives a mass-function index value of $\Gamma = -2.0 \pm 0.3$. This is consistent with the value of $\Gamma = -2.2 \pm 1.2$ obtained from a similar analysis of a well-observed B band luminosity function in M33 after a correction for the mass distribution of stellar aggregates in M33 is applied. Evidence is presented that the parent distributions establishing the stellar mass function derived from a galaxy-wide survey and that derived from a survey of a single aggregate system such as NGC 206 may have the same form. The brightest blue stars found in the NGC 206 survey were used to further investigate the usefulness of these objects as extragalactic distance indicators. It is concluded that the use of this secondary distance indicator may be extended to galaxies of types earlier than Sc by applying the method to the disk luminosity only rather than the total galaxy.

I. INTRODUCTION

Detailed investigations of rich OB associations provide information about massive-star formation. The observed luminosity function may be used to derive the frequency distribution of stellar masses in an association or cluster. Knowledge of such key physical characteristics as the spatial and mass distributions in a stellar aggregate will be essential to constraining models of the mechanisms and histories of massive-star formation in giant molecular clouds. Such studies will be valuable in refining the use of the luminous OB associations and blue supergiant stars as extragalactic distance indicators.

The very rich star cloud NGC 206, located in the southwest arm of M31 (hereafter referred to as the E6 arm), is a prime example of a large, massive OB association. The distance of M31, $\Delta = 652$ kpc (deVaucouleurs 1978), would seem to prohibit an extensive study of the stellar content of NGC 206. In fact, van den Bergh (1964) discovered that over 300 well-resolved stars in the association are brighter than apparent magnitude $B = 21.0$, which at the distance of M31 corresponds roughly to an absolute magnitude of $M_B = -4.0$. This implies a mass of $20\mathscr{M}_\odot$. Past investigations of the stellar mass spectrum in the high-mass range have been greatly hampered by the small number of massive stars in a single OB association or cluster. NGC 206, with its uncommonly high number of bright massive stars, provides us with a unique opportunity to study the stellar mass spectrum in the high-mass range, relatively free from adverse differential distance and extinction effects. In addition, it is highly probable that this association contains the brightest blue supergiant star in M31. Hence, information on the usefulness of the brightest blue stars as distance indicators may also be obtained from such an investigation.

II. OBSERVATIONAL MATERIAL

Photometric data for NGC 206 were obtained at McDonald Observatory with two high-quantum-efficiency area detectors at the $f/13.6$ Cassegrain focus of the 0.76 m reflector during two observing runs in December of 1982 and January of 1983. Images of the association in the U and B bands were taken with the Griboval electronographic camera (GEC) and in the B and V bands with the McDonald CCD camera. The photometric reduction of this material was accomplished using six photometric standards in the field measured by G. and A. de Vaucouleurs with the 2.1 m Struve reflector. The photoelectric magnitudes derived for these stars are given in Table III, in which each standard star is indicated by an asterisk. In addition, B and V magnitudes of NGC 206 stars from van den Bergh's study were used in a statistical comparison with the CCD and GEC photometry. The van den Bergh photometry, obtained from iris photometry of a plate made with the KPNO 2.1 m reflector under good seeing conditions, was also used to extend the BV photometry to fainter magnitudes as well as provide magnitude estimates for crowded stellar images which were impossible to study on the more poorly resolved images obtained at McDonald Observatory.

The Mark II version of the Griboval electronographic camera uses a 45 mm oxidized cesium-antimony photocathode which has a useful sensitivity from just beyond 6000 Å to well below the atmospheric cutoff at 3000 Å. The stream of photoelectrons from the cathode is magnetically focused onto a fine-grained electron-sensitive emulsion, Kodak Electron Image Film. Opal *et al.* (1982) have shown the areal response of a well-processed photocathode to be uniform to within 1% across the field, making flat-fielding procedures unnecessary for accurate photometry over modest areas of a

TABLE I. Plate material used in the photometric reductions.

Device	Filter	exp (s)	Airmass	Date
GEC	*B*	1200	1.11	12/6/82
GEC	*B*	1800	1.10	12/7/82
GEC	*B*	600	1.04	12/12/82
GEC	*U*	2400	1.60	12/6/82
GEC	*U*	3600	1.30	12/7/82
CCD	*B*	2100	1.57	1/11/83
CCD	*V*	1200	1.41	1/11/83
CCD	*B*	2100	1.79	1/12/83
CCD	*V*	1200	1.55	1/12/83

GEC plate. In addition, the transformation coefficients for converting the instrumental magnitudes to the standard Johnson *UBV* system have been found to be small and consistent among several cathodes. Pertinent data for the films selected for reduction in this study are given in Table I.

The photometric properties of the Texas CCD detector are similar to the type discussed by Leach (1980). Problems involved with the proper reconstruction of the true flux distribution on the sky, i.e., high readout noise, low resolution, variation of sensitivity across the detecting surface, and the high rate of cosmic-ray detection are offset by the promise of a detector which is extremely linear in its response over a large dynamic range. The detector in the Texas camera is a blue-sensitive RCA SID 52501 CCD (thinned, buried channel, backside illuminated). The sky-illuminated area is 512×320 pixels, resulting in a plate scale of 0.57 arcsec per pixel at the Cassegrain focus of the 0.76 m reflector. Pertinent data for the CCD images used in this study are found in Table I.

III. DATA REDUCTION

The process of extracting an accurate set of stellar magnitudes from the CCD or GEC images along with a reliable estimate of the photometric errors is complicated by a variety of problems such as nonlinear detector response and uneven sensitivity across the detecting area. With both instruments, before a stellar image in a crowded field may be integrated to yield a magnitude estimate one must ensure that the numerical values of the digitized image arrays are truly linear with the incident flux. In the case of GEC film reductions, the reduction process is further complicated by the introduction of systematic errors due to the PDS microdensitometer used to digitize the images.

The GEC films were scanned with the UT PDS microdensitometer using a 20 μm aperture and a step size of 20 μm. From many scans of a well-calibrated set of sensitometry spots, it was discovered that the response of the UT PDS becomes significantly nonlinear at photographic densities above $D = 1.5$ (where D is the density measured in a convergent beam). This nonlinear response was corrected for densities below $D = 3.0$ and an effort was made to measure only images having peak densities of less than $D = 2.0$ in order to ensure that the derived magnitudes would not depend greatly on the density correction. A series of plates having progressively longer exposure times were used to cover the magnitude range from $B = 14.0$ to $B = 19.5$, with the zero point being set from measurements of the bright standard stars on the short-exposure electronographs.

Following the method described by de Vaucouleurs (1984), stellar image density profiles of the photoelectric standards in the NGC 206 field were used to establish the relation between the photographic density values measured in the GEC images and the flux density incident on the detector. The response of the electronographic detector was found to be linear within 2% when the PDS instrumental signature is removed. In addition, magnitudes derived from simple integrations of the corrected PDS density arrays were found to be in tight agreement with photoelectrically derived B band magnitudes, confirming the linearity of the GEC response over an approximate magnitude range of four. Similar studies of the image profiles derived from the B and V CCD image data using the NGC 206 field standards, as well as image profiles of stars in M67 having photoelectrically derived magnitudes from Mendoza (1967), were conducted to confirm the high degree of linearity in the response of the McDonald CCD camera over a range of 6 mag. Magnitude derivations from stellar fields taken at several different chip locations showed that the effects of flat fielding and dark-frame subtraction were negligibly small in the magnitude range of interest, and hence those procedures were not used in the final reductions of the CCD frames.

The derivation of stellar magnitudes from the linear image arrays of NGC 206 was complicated by the fact that this rich cluster contains regions in which image crowding is severe. A high-quality CFH 4 m prime-focus plate taken under excellent seeing conditions, provided by R. Racine, was used to distinguish extremely tight groupings of stars which appeared as single stellar-like images on the lower-resolution CCD and GEC images. When available, magnitudes for the stars in these tight stellar groupings were taken from van den Bergh's photometry. High-resolution images taken under excellent seeing conditions with a quality linear detector will be needed in the future to extract stellar magnitudes in the tightest groupings in NGC 206. Even in the cases of well-resolved, single stellar images on the CCD and GEC images of NGC 206, the simple technique of simulated aperture integration is highly inadequate because of the flux contributed by the often prominent wings of neighboring stars. To reduce the effects of crowding, a point-spread-function (PSF) fitting method was adopted. With this technique, the mean stellar profile shape is determined empirically from several high-signal-to-noise, uncrowded images in a given frame. Each profile is reduced to a one-dimensional flux distribution by integrating the stellar image in successively larger concentric annuli. The sky background, taken to be the median value in an outer annulus, is subtracted from each of the mean annular integrations in the stellar image. In addition, the background algorithm rejects pixel values which exceed a specified level above the median sky value before final computation of the sky level, a feature which is important in the case of the crowded field of NGC 206. An integrated stellar magnitude m is obtained by determining the normalization factor k needed to fit the flux profile $f(r)$ of a program star to that of the empirically determined mean PSF, $\langle f(r) \rangle$:

$$\langle f(r) \rangle = kf(r), \tag{1}$$

$$k = \frac{\sum_{i=1}^{n} w(r) \left\{ \frac{\langle f(r) \rangle}{f(r)} \right\}}{\sum_{i=1}^{n} w(r)}, \tag{2}$$

where

$$w(r) = \left(\frac{S(r)}{N} \right)^2, \tag{3}$$

TABLE II. Linear equations used for transformation to Johnson system.

Equation	System
$(B-V)=(0.005\pm0.016)+(1.12\pm0.02)(b-v)_0$	CCD
$V=v_0-(3.11\pm0.02)+(0.06\pm0.02)(B-V)$	CCD
$B=b_0-(1.96\pm0.03)-(0.15\pm0.01)(B-V)$	GEC
$(U-B)=-(0.78\pm0.04)+(1.2\pm0.4)(u-b)_0$	GEC

and

$$m=C+2.5\log k. \qquad (4)$$

This method is effective because each profile point is weighted by the square of its predicted signal-to-noise ratio. In practice, the weighted mean value of k is determined from the k values determined by averaging the n profile points. The signal at each point $S(r)$ is estimated from a single Gaussian fit to the image profile, rather than the integrated value itself, in order to eliminate the adverse effects of noise fluctuation in the outer wings. The noise value N used in computing the signal-to-noise ratio at each point in the profile is taken to be the standard deviation of the pixel values integrated in a background annulus surrounding the image-profile region. The use of such a weighting scheme emphasizes the high-signal-to-noise core region of the stellar profile and, hence, is effective in analyzing the crowded regions of a stellar aggregate such as NGC 206. This technique was used to derive instrumental magnitudes with all of the GEC and CCD image arrays.

The instrumental magnitudes (ubv) were corrected for atmospheric extinction using mean coefficients and transformed to the standard UBV system of Johnson and Morgan (1953) via the usual linear expressions. The transformation coefficients determined from the NGC 206 field standards and the M67 standards of Mendoza are given in Table II. These values were determined from observations spanning several nights and are in excellent agreement with previous determinations.

The final catalog of UBV photometry for the brightest, well-resolved stars in NGC 206 is given in Table III. The coordinates given in Table III are in arcseconds with the Y axis approximately aligned in a north-south direction. A finding chart for several of the brightest stars measured on the CCD and GEC images is shown in Fig. 1 [Plate 15]. The surveyed NGC 206 region was taken to be a rectangular region measuring 3.0′×4.9′ centered on the system at $\alpha=0^h37^m47^s, \delta=+40°27'48''$ (1950.0). This area exceeds the rather ill-defined boundaries of the cluster and encompasses the photoelectric standards as well as a number of intermediate-color field stars. In the case of the B band pho-

TABLE III. A catalog of bright stars in NGC 206.

Name	X (arcsec)	Y (arcsec)	B	B − V	U − B
*1	232	268	18.00	1.34	1.38
2	239	246	19.77	0.40	
*3	249	241	15.78	0.64	−0.12
4	145	228	18.36	0.34	−0.40
5	264	225	19.37	0.09	
6	267	222	17.35	0.47	
7	157	211	18.68	−0.40	−0.82
8	169	205	17.42	−0.01	−0.55
9	122	201	18.79	0.28	0.14
10	167	201	17.71	−0.26	
*11	243	199	14.77	0.54	
12	171	198	16.03	−0.03	−0.70
13	137	197	18.83	0.18	
14	105	194	20.05	0.21	−1.05
15	269	194	17.87	0.74	
16	207	193	18.54	0.19	−0.11
17	169	191	18.54	0.29	
18	152	190	18.35	0.18	
19	134	188	18.89	−0.08	
20	151	186	19.46	0.14	
21	140	184	20.28	0.84	
22	152	183	17.07	−0.35	
23	166	183	19.10	0.57	
24	160	182	19.16	−0.16	
25	140	182	19.28	0.12	
26	168	180	18.36	0.00	
27	177	179	19.32	0.10	
28	233	178	19.46	0.18	−0.54
29	123	178	18.99	0.22	
30	167	177	18.67	0.04	
31	147	174	19.57	0.69	
32	150	174	17.85	−0.10	
33	263	174	20.18	1.14	
34	158	171	18.50	−0.27	
35	219	169	18.65	−0.25	−0.89
36	125	167	19.98	1.00	
37	182	166	18.15	−0.04	
38	139	164	17.95	−0.05	−0.90
39	253	163	19.14	0.27	
40	170	162	17.32	−0.30	
41	175	162	18.37	−0.13	
42	163	161	17.87	1.24	
43	256	160	19.14	0.23	
44	153	160	19.26	−0.03	
45	147	159	19.36	0.16	
46	168	159	19.37	0.33	
47	231	158	18.83	0.02	
48	242	157	20.77	1.84	
49	177	157	19.53	0.51	
50	230	155	19.23	−0.02	
51	234	154	18.61	−0.09	
52	224	153	19.22	−0.03	
53	177	152	19.52	0.11	
54	171	150	17.69	0.09	−0.48
55	133	150	19.16	−0.03	−1.25
56	202	150	19.18	−0.07	
57	152	149	18.97	−0.01	−0.64
58	185	149	18.13	−0.01	−0.65
59	150	149	19.21	0.01	
60	195	148	17.25	0.13	−0.68
61	159	143	18.13	0.97	
62	248	142	20.10	0.16	−0.92
63	215	141	19.05	0.02	−0.78
64	256	140	18.20	0.46	
65	181	138	18.43	−0.25	−0.98
66	133	137	19.80	0.81	
67	174	137	19.10	0.27	−0.45
68	190	135	18.15	0.02	−0.04
69	128	134	18.98	0.09	−0.78
70	147	133	19.07	−0.82	−0.36
71	229	133	18.37	−0.11	−0.90
72	215	128	18.18	−0.08	−0.54
73	183	128	18.87	0.05	
74	154	125	19.40	0.23	
75	126	121	20.38	1.24	
76	234	119	19.67	−0.28	−1.32
77	145	119	16.06	0.94	0.81
78	179	116	19.04	0.21	
79	170	115	19.19	0.21	
80	248	114	18.91	0.10	

1987AJ.....93..310O

TABLE III. (continued)

Name	X	Y	B	B − V	U − B	Name	X	Y	B	B − V	U − B
	(arcsec)						(arcsec)				
81	174	113	18.73	−0.09		116	202	64	20.74	1.54	
82	207	112	17.99	0.06	−1.16	117	164	62	18.78	−0.17	
83	199	111	19.21	0.03	−1.30	118	189	60	17.81	0.50	
84	180	108	18.37	0.08	−0.50	119	174	60	15.50	0.64	−0.01
*85	287	108	16.62	1.01	0.53	120	167	60	20.76	1.94	
86	191	107	18.90	0.40		121	207	56	20.15	0.64	0.10
87	145	101	18.69	0.76		122	221	55	19.63	0.05	
88	297	100	19.22	0.94		123	260	54	20.27	0.90	
89	146	98	18.24	0.42		124	150	53	19.73	0.59	
90	162	98	18.97	−0.01		125	90	52	17.32	0.87	0.42
91	167	97	18.51	−0.09		126	144	51	20.09	1.00	
92	215	96	20.27	1.64		127	186	50	19.57	0.25	
93	151	93	18.89	0.01		128	188	47	18.78	−0.03	
94	173	90	18.80	−0.05		129	145	46	18.17	0.01	−1.10
95	131	89	20.05	0.85		*130	231	45	15.34	0.64	0.00
96	138	86	18.75	0.56		131	207	42	19.05	0.81	0.26
97	153	85	17.68	0.05		132	181	42	19.72	0.35	
98	150	85	19.27	0.50		133	297	41	16.27	0.57	
99	188	85	19.46	0.40		134	174	38	18.88	0.72	
100	160	85	19.17	−0.20		135	171	36	19.15	0.01	
101	123	83	17.98	0.98	1.06	136	171	36	20.76	1.94	
102	89	81	19.18	0.52		137	175	34	18.96	−0.13	
103	96	79	19.31	1.24		138	296	31	19.31	0.34	
104	124	77	19.89	0.64		139	192	30	19.60	0.79	
105	222	76	19.93	0.90		140	215	29	19.68	−0.08	−0.33
106	126	75	19.57	0.50		141	186	26	19.17	−0.08	−1.12
107	126	74	18.72	0.13		142	151	25	17.87	1.06	1.09
108	114	72	18.76	0.49	0.73	143	169	23	19.09	0.11	
109	160	72	18.75	−0.05		144	211	23	18.01	0.03	−0.82
110	128	70	18.05	0.03		145	175	23	16.97	−0.38	
111	138	70	18.43	0.19		*146	105	19	17.17	0.83	0.16
112	133	67	17.30	0.49		147	170	19	19.41	0.00	
113	161	66	18.77	−0.04		148	202	19	19.25	0.30	
114	197	64	17.87	−0.10	−0.99	149	240	18	15.70	0.75	0.20
115	139	64	18.03	−0.41		150	267	5	16.22	0.61	

Note to TABLE III

Asterisk indicates standard star.

tometry listed in Table III, the values represent weighted means of magnitudes derived from the CCD and GEC images as well as values taken from the van den Bergh data set in cases of crowded stellar images. Small scale and zero-point corrections were applied to the GEC and van den Bergh data to transform all data sets to a mean system defined by the CCD data before computing final mean values. The photometric errors for each B band set were objectively derived through a statistical comparison between the three independent sets following the method of de Vaucouleurs and Head (1976). The interpolation curves of Fig. 2 were established to predict the photometric error and statistical weight of a magnitude estimate from a given set. Similar interpolation curves were fitted to the U and V error distributions, but in these cases only two independent data sets were available for each bandpass.

IV. REDDENING DETERMINATION

A reliable determination of the total extinction A_B and color excess $E(B-V)$ in NGC 206 was critical for a proper correction to an absolute-magnitude scale. The mean color excess $\langle E(B-V)\rangle$ across NGC 206 was determined initially by modeling the stellar color distribution in the association and fitting it to the observed distribution. Color-distribution models for the $B-V$ index in an OB association were assumed to roughly follow a $B-V$ distribution for the

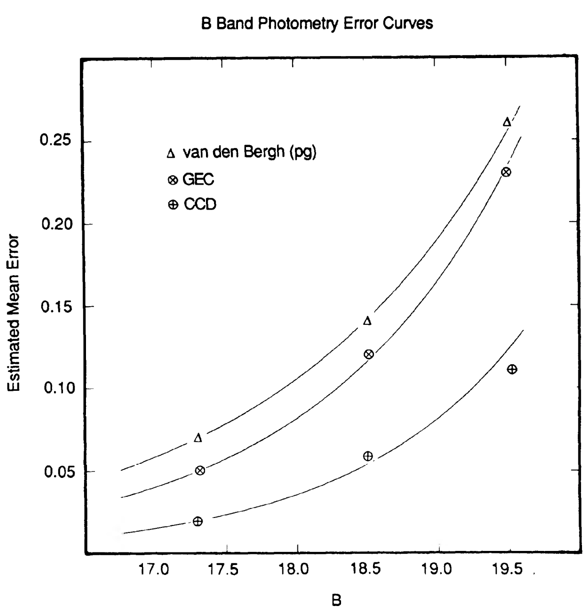

FIG. 2. Solid curves represent the interpolation formulas used to predict errors of magnitude estimates from each of the three independent sources of photometry: (1) electronograph, (2) CCD, and (3) van den Bergh (1964).

main sequence of a young cluster. Reddening-corrected cluster color-magnitude diagrams, empirically derived by Harris (1976) using high-precision photoelectric data, were used to compute color-distribution models for stellar aggregates having ages of 4×10^6 yr and 10^7 yr in order to bracket the expected age of NGC 206. These model color distributions were then smoothed with a Gaussian smoothing function having a standard deviation equal to the estimated mean error of the color-index values, $\sigma(B-V)=0.24$. The amount of shift in $B-V$ required to best fit the observed color distribution with the smoothed model distribution was taken as the color excess $\mathrm{E}(B-V)$. This method produced mean reddening values of $\langle\mathrm{E}(B-V)\rangle=0.30\pm0.07$ and $\langle\mathrm{E}(B-V)\rangle=0.23\pm0.07$ for assumed mean cluster ages of 4×10^6 and 10^7 yr respectively.

As a means of checking the $\mathrm{E}(B-V)\rangle$ value determined in the above manner, and also of estimating the degree of differential extinction present throughout NGC 206, the Q method of Johnson and Morgan was employed. The reddening-independent parameter Q was computed for each star in the survey which had U, B, and V measurements. Of this set, only estimates from bright, well-resolved images having $Q<-0.13$ were used to predict unreddened color values $(B-V)_0$ using the empirical relation $(B-V)_0=0.332Q$ (Johnson 1958). Hence, values of $\mathrm{E}(B-V)$ were computed throughout the OB association using the observed $B-V$ colors and the predicted reddening-free colors. The values of $\mathrm{E}(B-V)$ and their estimated errors determined by these two independent methods are shown in Table IV. As a further check, a mean color excess of $\langle\mathrm{E}(B-V)\rangle=0.30\pm0.05$ was predicted by using the formulas and data given in the RC2 (de Vaucouleurs, de Vaucouleurs, and Corwin 1976) to correct for galactic extinction and inclination effects. An internal extinction of $A_B=0.17$ was assumed for the disk of M31. All of the predicted $\mathrm{E}(B-V)$ values were found to be in reasonably good agreement and no statistically significant evidence for differential extinction in the surveyed NGC 206 region was present. Final weighted mean values of $\mathrm{E}(B-V)=0.27\pm0.03$ and $A_B=1.15\pm0.13$ were adopted for use in this study. An independent estimate of $\mathrm{E}(B-V)=0.45\pm0.2$ by Efremov and Ivanov (1984), using photographic photometry, is not in serious disagreement with the results given here considering the large error attached to their value. Some of the disagreement may be attributed to the fact that the EI survey extended over a larger region of the E6 arm, and hence may be more severely affected by the prominent dust lane on the inner edge of this spiral arm.

TABLE IV. Color-excess determinations in NGC 206.

Method	$\mathrm{E}(B-V)$	Error	A_B
1a	0.30	0.07	1.27
1b	0.23	0.07	0.97
2	0.29	0.03	1.23
3	0.23	0.04	0.97
mean	0.27	0.03	1.15

Notes to TABLE IV—Methods

1a = Fitting color distribution for cluster of age $T=4\times10^6$ yr.
1b = Fitting color distribution for cluster of age $T=10^7$ yr.
2 = Q method using bright, uncrowded stellar images.
3 = Calculated with data and standard formulas in RC2.

V. THE LUMINOSITY FUNCTION

The differential luminosity function $\phi(M_B)$, expressing the number of stars per unit magnitude interval as a function of absolute B magnitude, was derived from the NGC 206 B band photometry. Formally, the surface area of the surveyed region, defined here to be the $3.0'\times4.9'$ rectangular region centered on $\alpha=0^h37^m47^s$, $\delta=+40°27'48''$ (1950.0), should be included in the computation of $\phi(M_B)$, but this quantity was neglected since the computed value for each magnitude bin refers to the same area on the sky. The B magnitude data set was chosen for constructing the luminosity function because it was derived by combining three independent data sets (CCD,GEC,vdB) and included error estimates. The magnitude limit of the combined GEC and CCD B band surveys was estimated to be $B=19.5$. The vdB B band data, corrected for zero point by $B(\mathrm{CCD})-B(\mathrm{vdB})=-0.20$, were used to extend the luminosity function to a fainter magnitude. The V magnitude survey was used to compute colors for the bright, well-resolved stellar images, but was not suitable for constructing a complete V band luminosity function due to the lack of sufficient plate material.

The observed apparent luminosity function was derived by counting the number of stars in 0.5 mag bins over a magnitude range of $14.0\leqslant B\leqslant19.5$. The extreme bright end of the survey was composed of intermediate-color stars which were generally well displaced spatially from the main body of NGC 206. Since the surveyed region in NGC 206 was restricted to the area subtended by a single CCD frame, no significant background region could be defined for the purpose of directly estimating the field-star luminosity function. In addition, the lack of a complete V band survey allowed the construction of only a partially complete color-magnitude diagram. The observed color-magnitude diagram, shown in Fig. 3, was used to estimate the number of assumed field stars with $B-V\geqslant0.5$ at magnitude levels brighter than $B=18.0$ where incompleteness effects are held to a minimum. The number of these assumed field stars in each magnitude bin was compared to the counts predicted by the model of Bahcall and Soneira (1980) and found to roughly agree. Hence, the Bahcall and Soneira predicted field-star counts were subtracted from the observed apparent B band luminosity function as a means of isolating the NGC 206 population. It should be stressed that a more formal method of rejecting the field-star component using observed colors and some theoretical main-sequence track, as is done in Freedman's (1984) analysis, is more desirable. In this case, an extreme lack of completeness in the V band survey has prevented the adoption of such a method. The resulting luminosity function agrees reasonably well with that of van den Bergh to about $B=19.0$, the level at which crowding effects must become severe in both surveys. A comparison of the vdB B band luminosity function with that derived in this work was used to estimate the counting errors in each magnitude bin for $B\leqslant19.0$. The error bars established in this manner and shown in Fig. 4 do not include systematic errors in the counts from both surveys which surely exist to some degree due to incompleteness at progressively fainter magnitudes.

The mean B value in each bin of the apparent B band differential luminosity function was corrected for extinction with a value of $A_B=1.15$. Absolute magnitudes for each bin in the extinction-corrected function were computed with the geometric distance modulus of $\mu_0=24.07$ (de Vaucouleurs

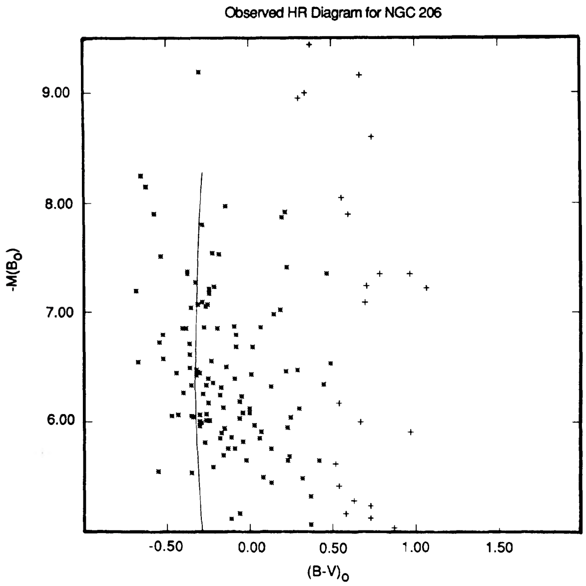

FIG. 3. Observed color-magnitude diagram is severely incomplete below $B = -18.5$ ($M_B = -6.7$). In addition, large errors in the V magnitudes, due to the lack of sufficient plate material, make use of the $(B-V)$ colors from faint stars unreliable. The brightest stars with $(B-V)_0 \geqslant 0.5$ were assumed to be field stars and are indicated by plus symbols. The number of field stars determined in this manner was found to agree sufficiently with the predicted counts of Bahcall and Soneira (1980). The solid line represents the blue edge of the upper end of the main sequence for a mean cluster of age $T = 4 \times 10^6$ yr from Harris (1976).

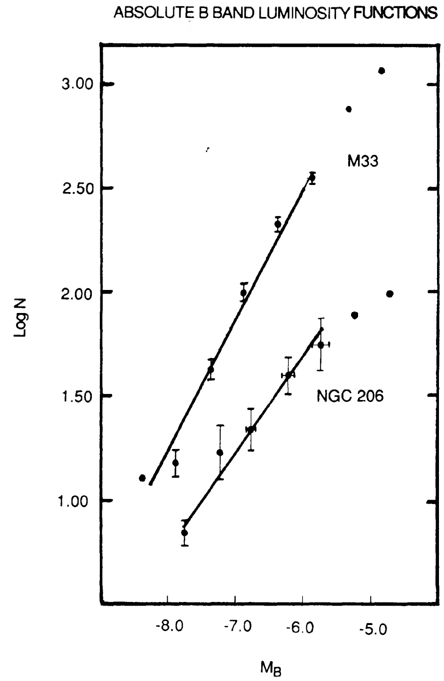

FIG. 4. The observed B band differential luminosity function for NGC 206 was obtained from a combination of the three independent data sets discussed in the text. The M33 function is taken from Freedman (1984). Weighted least-squares fits to these data were made in the range $-8.0 \leqslant M_B \leqslant -5.5$ to ensure that incompleteness at the faint end of the NGC 206 luminosity function would not be severe.

1978). The adopted absolute B band luminosity function $\phi(M_B)$ is plotted in Fig. 4 and tabulated in Table V.

A comparison between the NGC 206 luminosity function and the arbitrarily normalized M33 B band luminosity functions from Freedman (1984) is shown in Fig. 4 for the magnitude range covered in the NGC 206 survey. The results of weighted least-squares fits to each of these functions are shown in Table VI. The tabulated slope values α were derived from fits to n data points, each point representing a magnitude interval of 0.5. The total number of stars N used to construct the luminosity function H was large in the cases of Freedman's two M33 surveys in which the young stellar component was selected by $B-V$ and $U-B$ colors, respectively. The distance moduli for NGC 206 and M33 were taken from de Vaucouleurs (1978). The error attached to each slope estimate is simply the fitting error derived from a weighted least-squares fit. As these errors cannot account for possible systematic errors due to incompleteness, an effort was made to use only the brighter ends of the luminosity functions. A marked difference between the slopes of the luminosity functions from the two systems is apparent. Linear fits to two M33 B band luminosity functions for M33, derived by Freedman using various color-selection criteria, yield slope values around $\alpha = 0.64 \pm 0.05$ in an absolute-magnitude range similar to that surveyed in the NGC 206 study. The extensive V band luminosity functions of the extragalactic systems M33, Ho IX, NGC 300, and Leo A from Freedman (1985), based on surveys of large-reflector plates and CCD frames, agree well with one another in their slopes for the range $-9 \leqslant M_V \leqslant -4$. Similar studies of extragalactic dwarf systems by Hoessel, Schommer, and Danielson (1983) and Hoessel and Danielson (1984) in the B band yield an average slope of $\alpha = 0.55$ for the magnitude range $-9 \leqslant M_B \leqslant -5$. It is interesting to note that de Vaucouleurs (1956), using the Harvard star counts of Shapley (1931), found a similar slope for the stellar luminosity function in a region of the LMC which is dominated by extreme Population I stars. This area consists mainly of two large regions of approximately 2 square degrees each centered at $\alpha = 5^h38^m$, $\delta = -69°20'$ and $\alpha = 5^h30^m$, $\delta = -66°50'$. The stellar content of these regions, which comprise a large portion of the asymmetrical spiral arm of the LMC discussed by de Vaucouleurs (1954a,b), produces a roughly exponential luminosity function with a slope of $\alpha \approx 0.50$ in the range $-7.5 < M_B < -5.7$. Over the range $-5.0 < M_B < -2.0$, a purely exponential luminosity function of slope $\alpha = 0.43$ was determined. This value is very similar to that obtained in NGC 206, a pure Population I system. Although a thorough survey of these regions in the LMC should be repeated using modern techniques, it is of interest to note that two very similar slopes are obtained for two purely Population I systems. Comparing such studies with the result of this work, it seems that the NGC 206 luminosity function is marginally less steep in the range $-9 < M_B < -5.5$, with a slope of $\alpha = 0.47 \pm 0.03$, than any of the luminosity functions constructed from galaxy-wide stellar surveys.

In general, the galaxy-wide surveys are in close agreement with one another, a conclusion reached by Holmberg (1950) and confirmed by Freedman (1984), and are significantly steeper than the luminosity function of the single aggregate system NGC 206. In comparing these observations, one

TABLE V. Luminosity and mass functions in NGC 206.

B	$N(m \pm \Delta m/2)$	M_B	$\log \phi(B)$	$\log \mathscr{M}$	$\log F(\log \mathscr{M})$	$\log \xi(\log \mathscr{M})$	$\log T(\mathrm{yr})$
17.02	2	−8.2	—	—	—	—	—
17.48	7 ± 1	−7.74	1.15	1.91	1.87 ± 0.14	2.23 ± 0.21	6.64 ± 0.16
18.02	17 ± 5	−7.20	1.53	1.81	2.26 ± 0.18	2.57 ± 0.24	6.69 ± 0.16
18.48	22 ± 5	−6.74	1.64	1.73	2.37 ± 0.16	2.64 ± 0.22	6.72 ± 0.16
19.02	40 ± 8	−6.20	1.90	1.63	2.63 ± 0.15	2.86 ± 0.22	6.77 ± 0.16
19.50	56 ± 16	−5.72	2.05	1.54	2.77 ± 0.17	2.96 ± 0.24	6.82 ± 0.16
20.00	78	−5.22	—	—	—	—	—
20.50	99	−4.72	—	—	—	—	—

Notes to TABLE V

The $\mathscr{M}$-L and stellar lifetime data used to convert the observed NGC 206 B band luminosity function to the PDMF, $F(\log \mathscr{M})$, and the IMF, $\xi(\log \mathscr{M})$, were taken from Scalo (1986). A constant value of $|dM_B/d \log \mathscr{M}| = 5.3 \pm 1.5$ was used for the mass range investigated here.

must carefully consider the systematic effects on the slopes of the observed luminosity functions due to variations in the spatial resolutions of the surveys. Severe crowding effects will systematically cause the number of faint stars in a system to be underestimated, thereby reducing the slope of the observed luminosity distribution. Freedman (1983) has numerically modeled this systematic effect and finds that the error in the observed slope is between 15% and 35% when the number of merged images comprises 70%–85% of the photometric sample. If only half of the measured images are actually merged, the error in the observed slope is on the order of 5%. Hence, the slope difference between the NGC 206 function and the other galaxy-wide luminosity functions considered here, which exceeds 40%, must be real if the number of image mergers in the NGC 206 survey is not significantly greater than 50% of the sample. That this systematic difference is not the result of some resolution effect is supported by the fact that several of the extragalactic systems in the sample considered here have a distance similar to that of NGC 206 and hence should suffer the same systematic resolution effect. As will be considered presently in a derivation of the stellar mass frequency distribution in M33, this observed slope difference is most likely to be due to the fact that a galaxy-wide stellar survey is drawn from a distribution of stellar aggregates, each aggregate having its own upper stellar mass limit linked in some way to the total mass of the aggregate. Reddish (1978) was the first to note that the slope of the luminosity function derived from a galaxy-wide stellar survey should be systematically steeper than that of a single aggregate system observed under similar conditions, even if the mass frequency distributions of the two systems are dictated by the same initial stellar mass distribution law. Based on the data obtained in this work, and the fact that there is some theoretical basis for expecting a systematic slope difference between the luminosity functions of an entire galactic system and a single aggregate system such as NGC 206, I shall consider the observed slope variation between the NGC 206 function and the stellar luminosity functions from the galaxy-wide surveys considered here to be real and not the result of systematic errors in the photometry. A more detailed photometric survey of NGC 206 using higher-resolution-image material will be needed to check this conclusion.

VI. DETERMINATION OF THE IMF

Observational determinations of the mass distribution in a stellar system are needed to provide a fundamental constraint on theories of star formation. Also, knowledge of this distribution is a crucial ingredient in predicting the photometric evolution of a galaxy or in estimating a galaxy's present rate of star formation. Because a wide variety of analytical expressions for the stellar mass frequency distribution has been used in past works, a rigorous set of definitions is in order here. The mass spectrum $f(\mathscr{M})$ expresses the fraction of stars born per unit mass interval $d\mathscr{M}$ in a stellar system. In practice, it is more convenient to use the mass function $F(\log \mathscr{M})$, which expresses the fraction of stars born in a stellar system per unit logarithmic (base 10) mass interval. The following indices will be used in describing the shape of a stellar mass distribution:

$$\gamma(\mathscr{M}) = \frac{\partial \log f(\mathscr{M})}{\partial \log \mathscr{M}}\bigg|_{\mathscr{M}}, \tag{5}$$

$$\Gamma(\mathscr{M}) = \frac{\partial \log F(\log \mathscr{M})}{\partial \log \mathscr{M}}\bigg|_{\mathscr{M}}. \tag{6}$$

In the case of a power law mass function, Γ is a constant and is simply the numerical value of the slope of a line through the set of $[\log \mathscr{M}, \log F(\log \mathscr{M})]$ points. These indices are

TABLE VI. Slope estimates for the B luminosity function and IMF.

Object	α (LF)	n	N	Γ	$\mathscr{M}$ range	μ_0	A_B
NGC 206	0.47 ± 0.03	5	142	-1.96 ± 0.24	$1.5 \leqslant \log \mathscr{M} \leqslant 1.9$	24.07	1.15
NGC 206	0.49 ± 0.04	4	86	-2.20 ± 0.32	$1.6 \leqslant \log \mathscr{M} \leqslant 1.9$	24.07	1.15
M33 (a)	0.63 ± 0.05	5	340	-3.30 ± 0.30	$1.5 \leqslant \log \mathscr{M} \leqslant 1.9$	24.30	0.60
M33 (a)	0.74 ± 0.03	4	173	-3.76 ± 0.16	$1.6 \leqslant \log \mathscr{M} \leqslant 1.9$	24.30	0.60
M33 (b)	0.64 ± 0.05	5	168	-3.30 ± 0.40	$1.6 \leqslant \log \mathscr{M} \leqslant 1.9$	24.30	0.60
M33 (b)	0.69 ± 0.10	4	81	-3.51 ± 0.74	$1.7 \leqslant \log \mathscr{M} \leqslant 1.9$	24.30	0.60

Notes to TABLE VI

The NGC 206 luminosity function was constructed from the photometry in Table III. The M33 functions, taken from Freedman (1984), are constructed from (a) a B plate survey selected by $B-V$ colors, and (b) a B plate survey selected by $U-V$ colors. The distance moduli μ_0 were taken from de Vaucouleurs (1978). The NGC 206 A_B value used is the one derived in this work, and the M33 A_B value was taken from Freedman.

related by $\Gamma = \gamma + 1$. When $F(\log \mathscr{M})$ is computed directly from a photometric survey of a stellar system, as in this work, it is referred to as the present-day mass function (PDMF). Correcting this distribution for the stars which have died throughout the history of the system, we obtain the initial mass function (IMF), denoted as $\xi(\log \mathscr{M})$.

Direct determination of the mass frequency distribution in a stellar system is complicated by a variety of observational and theoretical problems. The consequences of theoretical uncertainties related to the effects of mass loss and convective overshoot in calibrating a mass-luminosity relation or in predicting stellar lifetimes, as well as the observational uncertainties due to low counting statistics and survey incompleteness, are thouroughly reviewed in Scalo (1986). Past determinations of the massive-star IMF by Miller and Scalo (1979), Garmany, Conti, and Chiosi (1982), Bisiacchi, Firmani, and Sarmiento (1983), and Humphreys and McKelroy (1984) have depended on catalogs of OB stars in the Galaxy and hence are highly subject to errors introduced by differential extinction, uncertainties in stellar distances, and differing metallicities. Attempts by Humphreys and McElroy to correct for incompleteness effects due to main-sequence evolution in OB star surveys in the Galaxy have improved the situation, but such studies are still subject to some of the aforementioned observational and theoretical uncertainties. The detailed survey of NGC 206 offers a large, homogeneous sample of massive stars having a common distance and extinction as well as, presumably, the same metallicity. Hence, a photometric survey between $M_B = -7.5$ and $M_B = -5.5$ of this extraordinary object provides us with a unique data set with which we may observationally determine the IMF in the very interesting mass range of $30\mathscr{M}_\odot < \mathscr{M} < 80\mathscr{M}_\odot$.

Following the photometric method of deriving an IMF outlined by Scalo, the absolute B band luminosity function $\phi(M_B)$, derived in the previous section, was transformed to an observed PDMF, $f(\log \mathscr{M})$, which expresses the number of main-sequence stars (i.e., in the core-hydrogen-burning stage) at mass $\mathscr{M}$ per unit interval of $\log \mathscr{M}$. The relation used for this transformation is as follows:

$$\xi(\log \mathscr{M}) = \phi(M_B)\left(\frac{d\ M_B}{d\ \log \mathscr{M}}\right). \tag{7}$$

The factor, $|dM_B/d\log \mathscr{M}|$, is the slope of the adopted mass-luminosity relation at mass $\mathscr{M}$. This relation, as stressed by Miller and Scalo (1979), should not relate the stellar luminosity on the zero-age main sequence to the mass, but rather must relate the average luminosity of hydrogen-burning stars of all ages at a given mass. This point is critical when using the $\phi(M_B)$ function in deriving a mass distribution, for it approximately compensates for the effect of brightening during the main-sequence stage. The $\mathscr{M}$-L relation used in this work, taken from Scalo, is a composite of observational determinations and theoretical predictions for massive-star $\mathscr{M}$-L relations taking into account the effects of stellar mass loss and convective overshoot. Because this relation was calibrated for the V band, a mean stellar color of $\langle B-V\rangle = -0.15$ was assumed for the NGC 206 sample in order that the tabulated M_V, $\log \mathscr{M}$ and $|dM_V/d\log \mathscr{M}|$ values could be applied to a B band scale, thereby allowing direct use of the observed luminosity function. The numerical values of the quantities used to transform the observed B band luminosity function to a mass distribution are given in Table V. The errors assigned to the tabulated $\log F(\log \mathscr{M})$ values were computed by propagating the error estimates for $\log \mathscr{M}$ and $|dM_B/d\log \mathscr{M}|$ as well as estimated counting errors in each bin of the observed B band luminosity function. Due to uncertainties in the mass-luminosity relation for massive stars, Scalo has estimated that a rather large uncertainty of ± 0.2 in $\log \mathscr{M}$, and an error of ± 1.5 in $|dM_B/d\log \mathscr{M}|$, is appropriate for the mass range considered here. The calculated PDMF is plotted in Fig. 5.

In order to derive the IMF from this distribution, one must know the relationship between stellar masses and stellar lifetimes as well as the stellar birthrate history in NGC 206. Herbig (1962) suggested that the stellar formation birthrate in giant molecular clouds was time dependent in the sense that lower-mass stars are formed early on, and the high-mass stars are formed later. When sufficiently massive stars are formed their large UV fluxes act to disperse the molecular cloud and curtail the star-formation process. Recent studies by Herbst and Miller (1983) and Stauffer (1980) have indicated that a large spread in ages of stars in young stellar aggregates must exist, in the sense that the least massive stars, still in the process of contracting onto the ZAMS, are much older than the most massive stars and the cluster age implied by the main-sequence turnoff. Doom *et al.* (1985) used theoretical evolutionary models which take

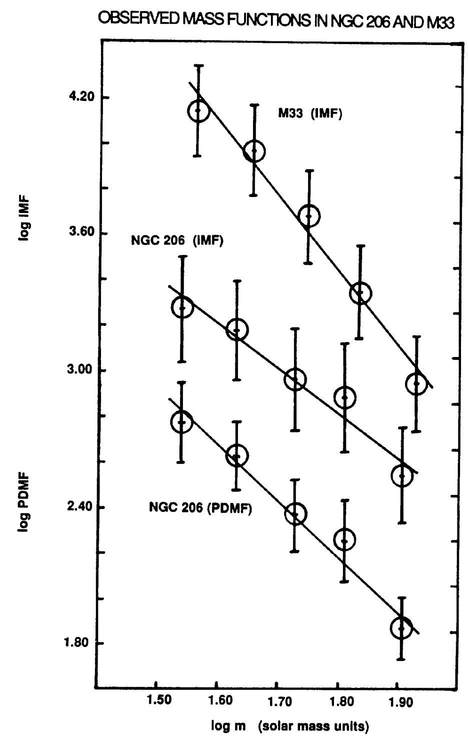

FIG. 5. The present-day mass function (PDMF) and the initial mass function (IMF) were derived from the NGC 206 data using the photometric method outlined by Scalo (1985). A linear fit to the IMF gives a mass-function index value of $\Gamma = -2.0 \pm 0.3$. Also shown is the apparent IMF in M33 obtained by transforming the B band luminosity function of Freedman. As discussed in the text, the slope of this distribution must be corrected to account for the mass distribution of stellar aggregates in M33 before obtaining a value of $\Gamma = -2.2 \pm 1.2$.

into account mass loss and convective overshoot to study the mass-age relationship in several OB associations. They find a definite mass-age relationship in the sense that more massive stars are formed as an association evolves (on a time scale of 15×10^6 yr). Elmegreen (1983) has pointed out that if a cloud forms stars following some IMF, then the stars form at random times with the most common masses occurring most of the time. Hence, a mass-age relation may be the result of a purely statistical effect. Because of the relatively small range in stellar lifetimes for the stars considered in this work, and the lack of any firm conclusion about the physical mechanisms governing the stellar birthrate history in a molecular cloud, I consider the birthrate to have been constant in NGC 206 since the time of formation of the least massive stars in the survey. With this assumption, calculation of the initial mass function is performed by dividing the value of the PDMF in each mass interval by the stellar lifetime appropriate to that mass. Since only the shape of the observed initial mass function $\xi(\log \mathscr{M})$ is to be considered, the results were arbitrarily normalized to an association age of $T=10^7$ yr. The values of the stellar lifetimes used in this calculation were taken from Scalo (1986), and the resulting $\log \xi(\log \mathscr{M})$ values and their estimated errors, are given in Table V and plotted in Fig. 5. Fitting the calculated IMF in the mass range of $1.5\leqslant\log \mathscr{M}\leqslant1.9$ gives a mass function index value of $\Gamma = -2.0\pm0.25$. The error estimate attached to this value reflects the fitting errors from a weighted least-squares solution in which the points have been weighted according to the error estimates tabulated in Table V. The weight of each point was established by propagating the counting errors in each bin of the luminosity function, and the estimated errors in $|dM_V/d\log \mathscr{M}|$ and the stellar lifetime T.

The extensive B band luminosity function of M33 from Freedman may be transformed to an IMF using this same method. This luminosity function was constructed from a survey of over 2600 stars chosen on the basis of their $B-V$ colors and hence should not suffer from large statistical uncertainties. The mass distribution obtained from a direct transformation of this function is shown in Fig. 5. As stated previously, the form of the mass distribution of stellar aggregates throughout a galaxy may significantly influence the form of the apparent stellar mass function derived from a galaxy-wide photometric survey. Vanbeveren (1984) has quantified this effect. Using the γ index defined in Eq. (5) (for the sake of clarity in referring to Vanbeveren's Eq. (18)) the apparent stellar mass spectrum $f_0(\mathscr{M})$ from a galaxy-wide sample of stars may be expressed as

$$f_0(\mathscr{M}) = C\mathscr{M}^{\gamma_0} = C\mathscr{M}^{\gamma_1(-\gamma-1)-1}. \quad (8)$$

Here γ_0 is the apparent mass spectrum index obtained from a direct transformation of a galaxy-wide stellar luminosity function, γ_1 is the index of the power law describing the mass frequency distribution of stellar aggregates in the galaxy, and C is a constant. An estimate of γ_1 was obtained by using the luminosity function of young star clusters in the LMC from Elson and Fall (1985) and assuming a constant mass-to-light ratio for the clusters. This gives a value of $\gamma_1 = -1.5\pm0.2$. Using the slope fitted to the M33 $\log \mathscr{M}$, $\log \xi(\log \mathscr{M})$ data of $\Gamma = -3.3\pm0.3$, the apparent index of the mass spectrum from the M33 stellar luminosity function is computed to be $\gamma_0 = (\Gamma-1) = -4.3\pm0.3$. These values of γ_1 and γ_0 can then be used, via Eq. (8), to compute the index γ of the true mass spectrum for the M33 stellar population surveyed. In this manner, a corrected value of $\gamma = -3.2\pm0.5$ was obtained from the M33 data. The error estimate attached to this value was obtained by propagating the estimated errors in γ_1 and γ_0. The resulting mass function index value of $\Gamma = -2.2\pm0.5$ agrees well with the NGC 206 value of $\Gamma = -2.0\pm0.25$. Admittedly, this result depends greatly on the *a priori* assumption that a value of γ_1 derived in the LMC is applicable in M33. Raising the error estimate attached to γ_1 to ±0.5, in order to account for possible differences between the LMC and M33 systems, raises the error attached to the corrected γ value to ±1.2.

Although the error estimates attached to the two Γ values derived here are large, it is interesting to note the similarity between these two independently derived values for the mass range $1.54\leqslant\log \mathscr{M}\leqslant1.9$. This result may add weight to the suggestion of Bisiacchi, Firmani, and Sarmiento ($\Gamma=-2.2$) and, later, Humphreys and McElroy ($\Gamma=-2.2$), that previous estimates in the range of $\Gamma\leqslant-1.5$ for massive stars were underestimations caused by incompleteness in the OB star catalogs used. It is disturbing that an aggregate correction to the BFS and HM estimates, similar to that used in the M33 mass-function analysis, will greatly lower their Γ values. This raises the question of just how applicable such a correction may be. Nevertheless, no such correction was applied to the NGC 206 data. In reality, the Γ value derived for NGC 206 should be considered an upper limit, since any revision to this estimate will probably steepen the IMF and increase the magnitude of the observed value of Γ due to the fact that the present survey must suffer from incompleteness at the faint end. Hence, it seems safe to conclude that the form of the mass function for the OB association NGC 206 is consistent with recent independent estimates of the form of the IMF for massive stars in the Galaxy and other nearby galactic systems.

VII. THE BRIGHTEST BLUE STARS AS DISTANCE INDICATORS

Use of the brightest blue stars in determining the distances of nearby, resolved galaxies has been discussed by Holmberg (1950), Sandage and Tammann (1974), de Vaucouleurs (1978), and Humphreys (1983). The theoretical study of Schild and Maeder (1983) has confirmed the correlation between the magnitude of the brightest star in a galaxy and the total luminosity of the galaxy. They have shown that this correlation may be attributed to purely statistical effects in the sense that more massive galaxies are statistically more likely to produce very massive stars. The calibration of the high-luminosity supergiant stars has thus far been restricted to galaxies having Hubble types of Sc and later. The application of this distance indicator in earlier-type galaxies is hampered by the heavy background intensity of the central spheroid and underlying exponential disk. Since it is very likely that the brightest blue stars of M31 reside in NGC 206, the photometric data collected in this study may be used to investigate the use of the brightest blue star calibration in an Sb spiral galaxy. In addition, information on the brightest stellar members in galaxies covering a wide range of Hubble types and luminosities will help to resolve the question of whether or not all galaxy luminosity functions are the same, or whether the upper mass limit of stars in a galaxy is determined by special local processes.

The relations between the magnitude of the brightest blue star B_1^*, and of the mean magnitude of the three brightest stars $\langle B^*\rangle_3$ and the face-on total absolute magnitude of the parent galaxy $M_T^0 = B_T^0 - \mu_0$, have been given by de Vaucouleurs (1978):

$$M_1^*(B) = 10.0 - 0.350(M_T^0 + 20.0)\ , \qquad (9)$$

$$\langle M^*\rangle_3(B) = 10.0 - 0.375(M_T^0 + 20.0)\ . \qquad (10)$$

Because the above relations were calibrated for revised Hubble types of Sc and later, the integrated magnitude M_T^0, is dominated by the flux from the exponential disk and the spiral arms. The flux contributed by the considerable bulge component of an Sb galaxy, such as M31, should cause an overestimation of the luminosity of the brightest star if the total integrated magnitude of the galaxy is used in the above relations. A recent study of the systematics of bulge-to-disk ratios by Simien and de Vaucouleurs (1986, hereafter referred to as SV), reveals that the bulge in an Sc galaxy contributes just under 10% of the total light, but the bulge in an Sb galaxy contributes over 20% to the total light of the galaxy. In order to determine the proper integrated quantity to be used in the brightest blue star calibration, several bright-star magnitude estimates were calculated for several possible choices for the M_T^0 quantity: (i) the integrated magnitude of the entire galaxy, (ii) the integrated magnitude of the old-disk component, (iii) the integrated magnitude of the spiral arm component, (iv) the integrated magnitude of the entire disk (old disk + arms), and finally (v) the integrated magnitude of NGC 206 alone. These predicted bright-star magnitudes were compared with the observed values of $B_1^* = 16.03$, the magnitude of the brightest blue star, and of $\langle B^*\rangle_3 = 16.78$, the mean magnitude of the three brightest stars, using a distance modulus of $\mu_0 = 24.07$ and total-extinction correction of $A_B = 1.15$.

In order to carry out this investigation the integrated magnitudes of the disk and spiral arms in M31 had to be computed. For this purpose, decompositions of the major- and minor-axis profiles of M31 were performed. Using the B band luminosity profiles of M31 from de Vaucouleurs (1958), the photometric parameters of the $r^{1/4}$ spheroid and the exponential disk were determined. The integrated magnitude of the old-disk component was found to be B_T(old disk) = 5.14, and the integrated magnitude of the spheroid was found to be B_T(spheroid) = 5.52. It should be noted that this fit excludes the flux contributed by the spiral arms. Using the derived integrated magnitudes for the spheroid and old-disk components and the total integrated magnitude for M31 of B_T(M31) = 4.36 ± 0.02 from de Vaucouleurs (1958), a value of B_T(arms) = 6.29 was computed for the integrated magnitude of the spiral arm component. Using the expressions given in RC2, face-on, extinction-corrected values of B_T^0(M31) = 3.59, B_T^0(old disk) = 4.37, and B_T^0(arms) = 5.52 were computed.

The above values correspond to a bulge-luminosity/total-luminosity ratio of $L_B/L_T = 0.34$, which differs somewhat from the corresponding values of other authors. Whitmore and Kirshner (1981) have derived a value of $L_B/L_T = 0.18$. The details of the fitting procedures were not described in this work. The original decomposition of the M31 luminosity profile by de Vaucouleurs was marred by numerical errors. A revision of this work by SV resulted in a value of $L_B/L_T = 0.55$. The large discrepancy between all of these derivations probably has to do with the particular details of each fitting procedure. The attempt at fitting only the old-disk component in this work may have caused an underestimation of the flux in the intermediate region of M31 where the flux contributions from the bulge and the disk are comparable. Hence, this decomposition could underestimate the strength of the bulge. Because of this fact, the SV decomposition was used to compute a second independent set of integrated magnitudes for the old-disk component and the spiral arm component. The value of B_T^0(arms) was derived by assuming that 20% of the total disk luminosity was due to the spiral arm component (Holmberg 1958). As with the values derived in this work, the SV values were corrected to extinction-free, face-on quantities. Fortunately, the integrated disk quantities of SV and those derived in this work are not radically different. Finally, using the aperture photometry of Corwin (private communication), the integrated magnitude for NGC 206, corrected for galactic and internal extinction as well as for the flux contributed by the underlying disk, was computed to be B_T^0(NGC 206) = 10.77. Using these integrated magnitude estimates in the brightest blue star calibrations given above, a variety of $M_1^*(B)$ and $\langle M^*\rangle_3(B)$ values were computed and the results are given in Table VII. Approximate error estimates for the calculated $M_1^*(B)$ and $\langle M^*\rangle_3(B)$ values are $\sigma(M_1^*) = \pm 0.6$ and $\sigma(\langle M^*\rangle_3) = \pm 0.35$.

Use of the total integrated magnitude of M31 results in an overestimation of the luminosities of the brightest blue stars. As expected, the results of these calculations indicate that the flux contributed by the bulge component has no significant effect upon the magnitude of the brightest blue star. The best agreement between the observed and predicted values for the brightest star is obtained by using the integrated magnitude of the spiral arm component. The integrated arm quantity from the SV decomposition gives the best agreement. The integrated arm component derived in this work gives the second best agreement. The integrated old-disk luminosity gives the next best agreement. Using the integrated magnitude of NGC 206 itself gives the poorest agreement.

The results of this exercise depend greatly on the assumption that the brightest blue star in M31 is really in NGC 206. From inspections of full-field photographs of M31, this would seem to be a reasonable assumption. Also, the star counts of Seyfert and Nassau (1946) confirm that the brightest stars of M31 are found approximately between $B = 16.0$ and $B = 16.5$. If a brighter blue star does exist outside of NGC 206, then the integrated disk magnitude would probably give the best fit. The fact that the best agreement for the $\langle M^*\rangle_3(B)$ estimate was obtained by using the integrated spiral arm magnitude may argue against the choice of the disk value, but here again we must make the *a priori* assumption that the three brightest blue stars of M31 reside in NGC 206. Consequently, the results of the $\langle M^*\rangle_3(B)$

TABLE VII. Predicted brightest blue star magnitudes.

Quantity	Source	B_T^0	M_T^0	$M_1^*(B)$	$\langle M^*\rangle_3(B)$
M31 (total)	1	3.59	− 20.48	− 10.17	− 10.06
old disk	2	4.37	− 19.70	− 9.90	− 9.77
spiral arms	2	5.52	− 18.55	− 9.49	− 9.34
old disk + arms	3	4.42	− 19.65	− 9.88	− 9.75
spiral arms	3	6.94	− 17.13	− 9.00	− 8.80
old disk	3	4.66	− 19.41	− 9.79	− 9.66
NGC 206 (total)	2	10.77	− 13.30	− 7.66	− 7.37
Observed				− 9.19	− 8.44

Notes to TABLE VII

The sources of the integrated B band magnitudes, in most cases derived from profile decompositions, are: (1) RC2, (2) Odewahn, (3) Simien and de Vaucouleurs. Propagating the estimated errors of the integrated quantities and the errors of the coefficients in the bright-star relation, the estimated error of any M_1^* (1) value is approximately ± 0.6 mag.

calculations are subject to revision when exhaustive stellar photometry in M31 becomes available. The result that the spiral arm magnitude gives the best predicted value is not surprising since the spiral arms are the sites of massive-star formation. The results of this investigation confirm the notion that the total integrated magnitude of an early-type galaxy such as M31 is not the proper quantity for use in predicting the brightest-star magnitude and imply that proper correction for bulge luminosities in galaxy types earlier than Sc will be important in refining the use of the brightest blue stars as extragalactic indicators.

VIII. SUMMARY

A detailed *UBV* photometric survey of the stellar content of the rich OB association NGC 206 has been carried out with two high-quantum-efficiency area detectors. A careful analysis of the photometric errors has allowed the derivation of weighted mean *B* band magnitudes, from which a differential luminosity function has been constructed. This luminosity function was transformed to an absolute scale using the estimated total absorption value of $A_B = 1.15 \pm 0.13$ and a geometric distance modulus of $\mu_0 = 24.07$.

With a method which utilizes photometric data alone, the well-observed *B* band luminosity function for NGC 206 was transformed to a present-day mass function. Assuming a constant birthrate since the formation of the least massive stars in the survey, and using stellar lifetime estimates which take into account the significant effects of mass loss and convective overshoot, an initial mass function was derived from the NGC 206 data. A power law fit to this IMF gives a mass-function index value of $\Gamma = -2.0 \pm 0.3$. This value is consistent with several independent determinations of the slope of the IMF for massive stars ($20\mathscr{M}_\odot \leqslant \mathscr{M} \leqslant 100\mathscr{M}_\odot$). Of some significance is the fact that the same transformation method, when applied to Freedman's extremely well-observed *B* band luminosity function in M33, gives the similar value of $\Gamma = -2.2 \pm 1.2$ when the proper correction is made for the mass distribution of stellar aggregates in M33. Rigorous application of this aggregate correction is questionable. Freedman (1986) has observed that the form of the luminosity function in M33 is closely reproduced in a number of other galactic systems, indicating the possible existence of some universal initial mass function. The observational results presented here would indicate that the parent distributions establishing the forms of the mass functions in galaxy-wide systems and in single aggregate systems such as NGC 206 must not differ significantly in the high-mass regime.

The brightest blue stars discovered in NGC 206 were used to study the use of such objects as extragalactic distance indicators. Using the brightest blue star relations of de Vaucouleurs (1978), and a number of M31 luminosity-profile decompositions giving integrated magnitudes for the old-disk and spiral arm components, the observed brightest blue star values were used to determine which integrated luminosity is the most appropriate for use in the bright-star relation. As is shown in Table VII, the brightness of the most massive star was found to be correlated most strongly with the integrated magnitude of the spiral arms and somewhat less with the integrated old-disk luminosity. The conclusion is that proper consideration of bulge luminosities may be an important step in refining the use of the brightest blue stars as extragalactic distance indicators.

The author is indebted to G. de Vaucouleurs for his unfailing guidance and encouragement. In addition, many interesting conversations with J. Scalo were crucial to the completion of this work.

REFERENCES

Bahcall, J. N., and Soneira, R. M. (1980). Astrophys. J. Suppl. **44**, 73.
Bisiacchi, G. F., Firmani, C., and Sarmiento, A. F. (1983). Astron. Astrophys. **119**, 167.
de Vaucouleurs, G. (1954a). Observatory **74**, 23.
de Vaucouleurs, G. (1954b). Observatory **74**, 158.
de Vaucouleurs, G. (1956). Ir. Astron. J. **4**, No. 1, 13.
de Vaucouleurs, G. (1958). Astron. J. **128**, 465.
de Vaucouleurs, G. (1978). Astrophys. J. **224**, 14.
de Vaucouleurs, G., and Head, C. (1978). Astrophys. J. Suppl. **36**, 439.
de Vaucouleurs, G. (1984). In *Astronomy with Schmidt-Type Telescopes*, IAU Colloquium No. 78, edited by M. Capaccioli (Reidel, Dordrecht), p. 367.
de Vaucouleurs, G., de Vaucouleurs, A., and Corwin, H. G. (1976). *The Second Reference Catalog of Bright Galaxies* (University of Texas, Austin).
Doom, C., DeGrave, J. P., and de Loore, C. (1985). Astrophys. J. **290**, 185.
Effremov, Y. N., and Ivanov, G. R. (1984). Astron. Tsirk. **1352**, 1.
Elmegreen, B. G. (1983a). In *The Nearby Stars and the Stellar Luminosity Function*, IAU Colloquium No. 76, edited by A. G. Davis Philip and A. R. Upgren (Van Vleck Observatory, Schenectady), p. 235.
Elson, R., and Fall, S. (1985). Publ. Astron. Soc. Pac. **97**, 692.
Freedman, W. L. (1983a). In *The Nearby Stars and the Stellar Luminosity Function*, IAU Colloquium No. 76, edited by A. G. Davis Philip and A. R. Upgren (Van Vleck Observatory, Schenectady), p. 191.
Freedman, W. L. (1984). Ph.D. dissertation, University of Toronto (unpublished).
Freedman, W. L. (1985). Astrophys. J. **299**, 74.
Garmany, C. D., Conti, P. S., and Chiosi, C. (1982). Astrophys. J. **263**, 777.
Harris, G. L. (1976). Astrophys. J. Suppl. **30**, 451.
Herbig, G. H. (1962). Astrophys. J. **135**, 736.
Herbst, W., and Miller, D. P. (1982). Astron. J. **87**, 1478.
Hoessel, J. G., and Danielson, G. E. (1984). Astrophys. J. **286**, 159.
Hoessel, J. G., Schommer, R. A., and Danielson, G. E. (1983). Astrophys. J. **274**, 577.
Holmberg, E. (1950). Lund. Medd. (II) **128**, 38.
Holmberg, E. (1958). Lund. Medd. (II) **136**, 1.
Humphreys, R. M. (1983) Astrophys. J. **269**, 335.
Humphreys, R. M., and McElroy, D. B. (1984). Astrophys. J. **284**, 565.
Johnson, H. L., and Morgan, W. W. (1953). Astron. J. **117**, 313.
Johnson, L. (1958). Lowell Obs. Bull. **4**, 37.
Leach, R. W. (1980). Publ. Astron. Soc. Pac. **92**, 233.
Mendoza, V. (1967). Bol. Obs. Tonantzintla Tacubaya **4**, 149.
Miller, G. E., and Scalo, J. M. (1979). Astrophys. J. Suppl. **41**, 513.
Opal, C. B., Bozyan, E. P., and Griboval, P. J. (1982). In *Instrumentation in Astronomy IV*, edited by D. L. Crawford (Society of Photo-Optical Instrumentation Engineers, Bellingham, WA), p. 1.
Reddish, V. C. (1978). In *International Series in Natural Philosophy, Stellar Formation* (Pergamon, Oxford), Vol. 97, p. 182.
Sandage, A., and Tammann, G. A. (1974). Astrophys. J. **191**, 603.
Scalo, J. (1986). Fund. Cos. Phys. (in press).
Schild, H., and Maeder, A. (1983). Astron. Astrophys. **127**, 238.
Seyfert, C. K., and Nassau, J. J. (1946). Astrophys. J. **101**, 179.
Shapley, H. (1931). Harv. Bull. No. 881, 4.
Simien, F., and de Vaucouleurs, G. (1986). Astrophys. J. **302**, 564.
Stauffer, J. R. (1980). Astron. J. **85**, 1341.
Vanbeveren, D. (1984). Astron. Astrophys. **139**, 545.
van den Bergh, S. (1964). Astrophys. J. Suppl. **9**, 65.
Whitmore, B. C., and Kirshner, R. P. (1981). Astrophys. J. **250**, 43.

1987AJ.....93..310O

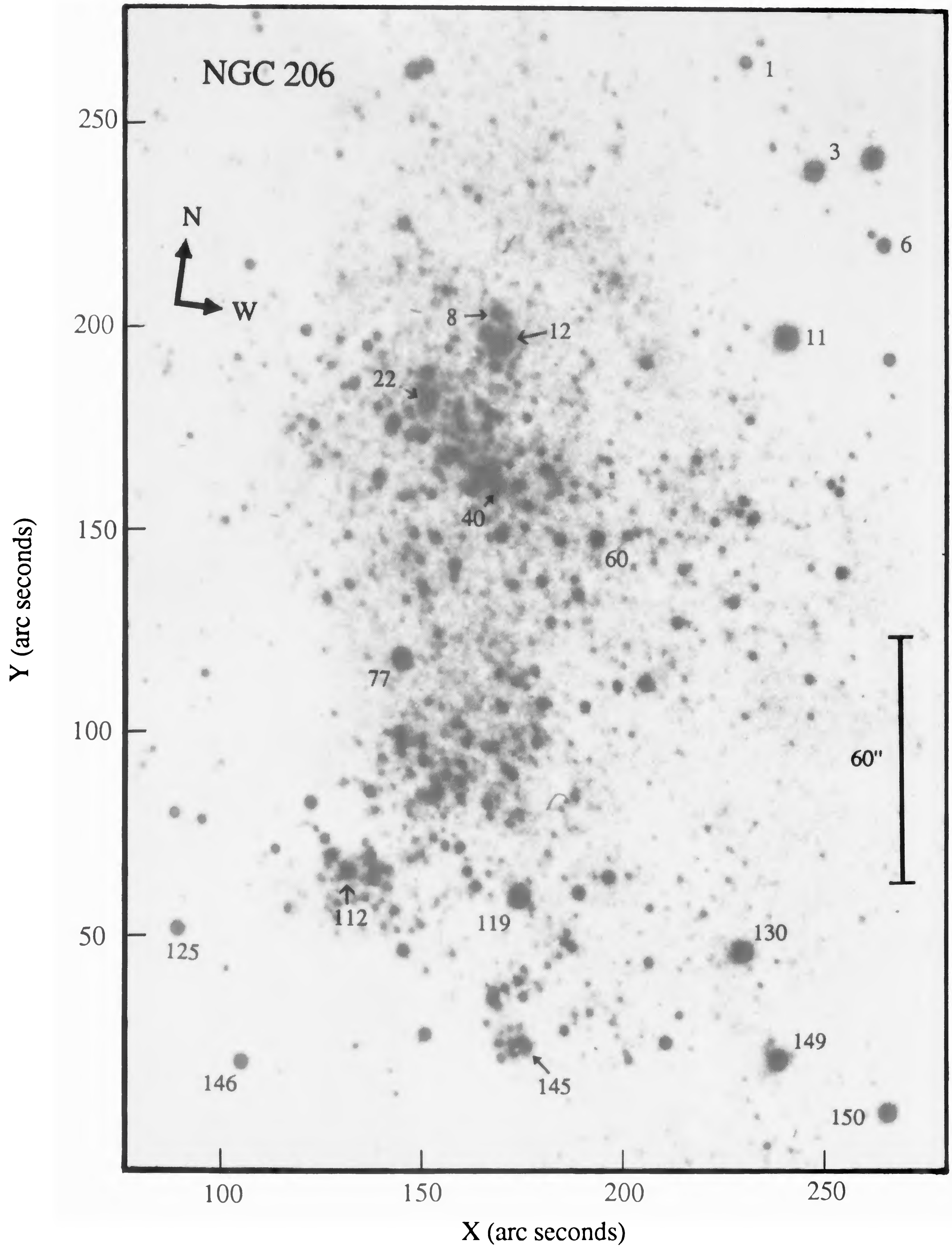

FIG. 1. A portion of a CFH 4 m prime-focus plate shows the NGC 206 region surveyed. The number designations for the labeled stars correspond to those in Table III.

Stephen Odewahn (see page 312)